Towards a Boundary Condition for Convective Wave Equation and Sound Diffraction at a Trailing Edge Inside a Flow

Drasko Masovic[1], Eugene Nijman[1], Jan Rejlek[1], Robert Höldrich[2]

[1] *Virtual Vehicle Research Center, 8010 Graz, E-Mails: drasko.masovic@v2c2.at, eugene.nijman@v2c2.at, jan.rejlek@v2c2.at*

[2] *IEM University of Music and Performing Arts Graz, 8010 Graz, E-Mail: robert.hoeldrich@kug.ac.at*

Introduction

Low frequency sound radiated from an open unflanged pipe is greatly affected by the attenuation at the trailing edge of the pipe [1] and the refraction in the mixing region of the jet, even at low mean flow velocities. Although the flow-acoustic coupling is generally weak, the vortices shed from the pipe edge are partly energized by the incoming sound wave and, thus, appear as an acoustic sink. The sound is then partly regenerated through the action of the vortices on the edge. Both sound attenuation and "generation" mechanisms are driven by the incoming acoustic wave, while the contribution of the mean flow is only through its abrupt but steady spatial changes close to the edge. Therefore, steady properties of the main flow are sufficient for estimation of sound propagation at low frequencies. Indeed, the combination of steady Reynolds-averaged Navier-Stokes (RANS) equations and Linearized Euler Equations (LEE) has been successfully used in literature for solving this type of problems [2-4].

Existing computational fluid dynamics (CFD) solvers, mostly based on low-order Finite Volume Method [5], are well optimized for the solution of Navier-Stokes equations and show remarkable efficiency and robustness. On the other hand, less common calculations of the acoustic propagation based on LEE are often associated with difficulties, such as large computational efforts and instability. Two alternative approaches are:

- solving a single (convective) wave equation and
- solving some form of aeroacoustic analogy.

The first approach most often requires a simplified model of the mean flow for estimation of sound propagation (left-hand side of the equation), such as uniform flow in the classical convective wave equation, or parallel shear flow in Lilley's equation [6]. Other details of the flow and its interaction with the acoustic waves have to be either neglected, which might lead to inaccuracies, or shifted to the right-hand side of the equation, to appear as the sound sources. The latter solution is in the basis of the second approach, which utilizes aeroacoustic analogies. Since the propagation effects are (at least partly) treated as artificial sources of sound, which are dependent on the solution of the acoustic problem, the analogy requires the following:

- expansion of the source region over the entire region in which the critical sound propagation effects take place, which can lead to very distributed "sound sources" and
- appropriate modelling of the flow-acoustic effects on sound propagation, which allows the assessment of such source terms.

Both prerequisites limit the applicability of aeroacoustic analogies in highly inhomogeneous flows.

Still, the analogies remain essential for characterisation of mechanisms of aerodynamic sound generation and, when used appropriately, can lead to very efficient calculations by means of single-unknown acoustic wave equations. In this work, we try to utilize different aeroacoustic analogies to estimate sound propagation around a trailing edge of a circular pipe with a flow. As a result, a form of convective wave equation with imposed vortex-induced acoustic sink effects will be used and compared with computationally more demanding system of Linearized Euler Equations.

Convective wave equation

In the following, we attempt to estimate the far-field directivity of an open pipe by numerically solving a single convective wave equation. We start with Phillips equation without mass, force, or heat sources and neglect the effects of viscosity and heat conduction (isentropic flow). We also assume the pressure perturbations of a perfect gas to be very small compared to the static value, which is also assumed to be constant ($p_0 = p_\infty = const$), so that the equation simplifies to:

$$\frac{D^2 p'}{Dt^2} - \nabla \cdot \left(c^2 \nabla p'\right) = \rho_\infty c_\infty^2 \left[\nabla \cdot \left(\mathbf{v} \cdot \nabla \mathbf{v}\right) - \mathbf{v} \cdot \nabla\left(\nabla \cdot \mathbf{v}\right)\right], \quad [\mathrm{Pa/s^2}] \qquad (1)$$

where p' denotes the pressure perturbation and $\mathbf{v}$, ρ, and c denote velocity, density, and sound speed, respectively. Subscript $_\infty$ denotes a reference value at infinity, where the mean flow is quiescent. The left-hand side operator of this form of convective wave equation is capable of capturing sound propagation effects due to spatially varying mean flow velocity (inside the total derivative of the first term) and sound speed (the second term). Unfortunately, part of the sound propagation is still contained inside the right-hand side terms, as proven by Doak [7] for shear flows. In low Mach number flows, these terms become important only in the regions of abrupt changes of the mean flow velocity, such as at the trailing edge of a pipe with a flow. Moreover, the right-hand side of the equation can be expanded as:

$$\rho_\infty c_\infty^2 \left[\nabla \cdot \left(\nabla \frac{v^2}{2} + (\nabla \times \mathbf{v}) \times \mathbf{v} \right) - \mathbf{v} \cdot \nabla (\nabla \cdot \mathbf{v}) \right]. \qquad [\mathrm{Pa/s^2}] \qquad (2)$$

The term $\rho_\infty c_\infty^2 \nabla \cdot [(\nabla \times \mathbf{v}) \times \mathbf{v}] = \rho_\infty c_\infty^2 \nabla \cdot (\boldsymbol{\omega} \times \mathbf{v})$, with $\boldsymbol{\omega}$ denoting vorticity, points to the vortex-sound interaction and the dominant cause of the acoustic sink at the edge in low Mach number flows and at low sound frequencies [8]. Since the term also involves the acoustic velocity, which is part of the sought for solution, its calculation is not straightforward. To circumvent this, one can attempt to estimate the term prior to the acoustic calculation. The unsteady incompressible pressure at the pipe edge p_{ic}' is due to the action of the axial component of the Coriolis force on the pipe wall, so we can estimate it from [1]:

$$\frac{\partial p_{ic}'}{\partial x} \approx \rho_J (\boldsymbol{\omega} \times \mathbf{v})_x \approx \frac{\partial}{\partial x} (\rho_J v_J v_{ac}') \qquad [\mathrm{Pa/m}] \qquad (3)$$

as:

$$p_{ic}' \approx -\rho_J v_J \frac{2 p_{ac}'}{\rho_J c_J} = -2 M_J p_{ac}', \qquad [\mathrm{Pa}] \qquad (4)$$

where p_{ac}' and v_{ac}' are the acoustic perturbations of pressure and axial velocity component at the pipe opening, respectively, due to the incoming sound wave, subscript $_J$ denotes the values in the mean flow (jet), and M_J represents the local Mach number value. Here, the approximation $v_{ac}' \approx 2p_{ac}'/(\rho_J c_J)$ was used, since the reflection coefficient at the pipe opening is close to -1 at low frequencies and low Mach numbers, so both incoming and reflecting waves contribute nearly equally to the velocity perturbation. The resulting incompressible pressure has the opposite sign of the initial acoustic one, which implies that the sink at the edge is equal to $(-1-2M_J)p_{ac}'$. The reaction force of the edge is also the actual cause of the far-field dipole-like radiation outside the pipe, with the positive lobe at the pipe axis downstream.

Numerical solution

Phillips partial differential equation is solved using the first-order Finite Element Method (FEM). The two-dimensional mesh applied on the axisymmetric geometry is very simple and consists of quadrilateral elements with the dimensions 1cm x 1cm everywhere, except within the extension of the pipe wall, where the dimensions are 0.02cm x 1cm, match the thickness of the pipe wall. The pipe length is 68cm. The computational domain extends outside the pipe 50cm in both axial and radial directions from the pipe opening. As a result, the mesh consists of 5086 elements and 5306 nodes. Small size of the elements justifies the implementation of simple linear basis functions. The time step is 50µs. The main acoustic monopole source is placed at the half length of the pipe, 1cm from the axis in the radial direction, and the excitation signal is a sine wave. All boundaries are treated as rigid walls, with normal component of the pressure gradient equal to zero. The time-domain simulation is interrupted at the time $t = 2.5$ms in order to avoid the superposition of the reflections from the outer boundaries of the computational domain. The radiation patterns are estimated at the distance 34cm from the opening of the pipe, from the mean square values of the pressure perturbation within one half of the signal period. The mean flow properties are interpolated from the results of the CFD RANS simulations.

In the first calculation, the right-hand side of the Equation (1) is neglected. In the second calculation, the secondary aerodynamic source is approximated with the incompressible pressure perturbation according to the Equation (4). The acoustic pressure dependent sink at the pipe edge is imposed through the modification of the corresponding values of the stiffness matrix for the two nodes at the pipe edge. Figure 1 shows the distribution of the pressure perturbation p' at one time instant for both calculations. The maximum Mach number of the flow at the pipe axis is $M_{max} = 0.25$ and the maximum temperature is $T_{max} = 300$ºC. Frequency of the emitted sound is 1146Hz which corresponds to Helmholtz number $He = 0.3$.

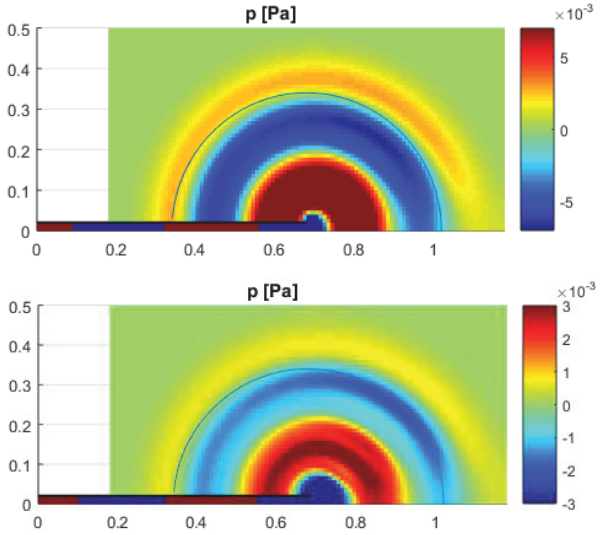

Figure 1: Distribution of pressure perturbation p' at one instant of time with the incompressible pressure perturbation (above) neglected, (below) approximated as $p_{ic}' \approx -2M_J p_{ac}'$; the blue lines represent the arc on which the radiation patterns are acquired.

The estimated radiation patterns are given in Figure 2 for the first (blue line) and the second calculation (red line) and for two sets of conditions:

- $M_{max} = 0.15$, $T_{max} = 41$ºC, $He = 0.5$ and
- $M_{max} = 0.25$, $T_{max} = 300$ºC, $He = 0.3$.

In both cases, the results are compared with the measurements after the normalization of the radiation patterns according to the total radiated power. Inclusion of the effect of the vortices, based on the vortex sound theory, improves the prediction of the far-field directivity even though a single convective wave equation is solved. The introduced additional condition at the pipe edge, a pressure dependent sink, can therefore be used for more accurate estimation of sound diffraction at the trailing edge. The

utilized approximations provide a good accuracy of the resulting field at low Mach number values. The accuracy drops at higher mean flow velocities, due to the neglected terms in the starting Phillips equation.

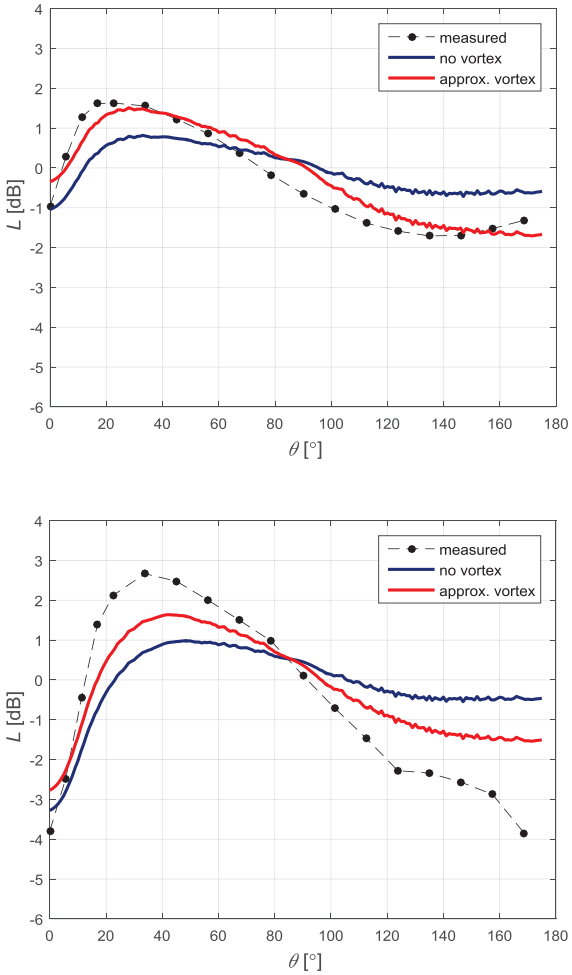

Figure 2: Estimated and measured radiation pattern shapes for: (above) $M_{max} = 0.15$, $T_{max} = 41$ºC, $He = 0.5$ and (below) $M_{max} = 0.25$, $T_{max} = 300$ºC, $He = 0.3$; blue lines represent the results with neglected incompressible pressure perturbation, red lines represent the resutls with approximated incompressible pressure perturbation; normalization is based on the total radiated power.

Comparison with Linearized Euler Equations

The conservative form of Linearized Euler Equations [3] will be used here to solve the same sound propagation problem in time domain. For a perfect gas ($\gamma p = \rho c^2$) without unsteady mass- or heat-sources, the system reads:

$$\frac{\partial \rho'}{\partial t} + \nabla \cdot (\rho \mathbf{v})' = 0, \qquad [\mathrm{kg/m^3 s}] \qquad (5)$$

$$\frac{\partial (\rho \mathbf{v})'}{\partial t} + \nabla \cdot (\rho \mathbf{v})' + \nabla \left(\frac{\gamma p_0}{p_{c0}} p_c' \right) = 0, \qquad [\mathrm{kg/m^2 s^2}] \qquad (6)$$

$$\frac{\partial p_c'}{\partial t} + \nabla \cdot (p_c \mathbf{v})' = 0, \qquad [\mathrm{1/s}] \qquad (7)$$

with $p_c = (p'/p_\infty)^{1/\gamma} = p_{c0} + p_c'$, $p_{c0} = (p_0/p_\infty)^{1/\gamma}$, and $p_c' = p_{c0} p'/(\gamma p_0) << p_{c0}$, where p_∞ is an arbitrary constant reference value of pressure (for example, static pressure in a quiescent flow at infinity, $p_\infty = 101$kPa). Therefore, p_c can be interpreted as a normalized pressure perturbation.

The system of Linearized Euler Equations in cylindrical coordinates is discretized and solved in time domain using the Discontinuous Galerkin Method (DGM). For this purpose, a two-dimensional triangular mesh was used. Typical dimension of the elements varies between 2mm (equal to the pipe wall thickness) within the extension of the pipe wall, around 1cm inside the pipe (with the inner radius 2cm) and its extension, up to around 8cm far from the edge of the pipe. The adapted mesh takes the advantage of the higher-order DGM and provides higher accuracy in the region of vortical flow, close to the edge. The total length of the pipe is 30cm and the exterior propagation region extends 50cm in both axial and radial directions from the pipe opening. The mesh consists of 570 elements with 10 interior and interface nodes each, for the third-order accuracy.

Source of the plane wave inside the pipe is introduced through the time varying pressure boundary condition at the upstream end of the pipe. As before, a sine-wave is used for simplicity. All other boundary conditions are set to rigid wall boundary condition, that is, normal components of the pressure and density gradients, as well as both components of the momentum equal zero, with the exception of the axial component of the momentum at the pipe axis, which is in general non-zero. Local Lax–Friedrichs flux is applied as the numerical flux at the interfaces between the elements [4], to support the discontinuity of the basis functions between the elements. In order to suppress the growing linear instability due to the vortex formation at the edge, artificial dissipation is added in the form of a two-dimensional exponential filter [9], which does not distort significantly the acoustic wave component.

Since no absorbing boundary conditions are introduced at the boundaries of the computational domain, the time-domain simulations are interrupted before the first reflections reach the control points where the radiation patterns are estimated. The equidistant points are set along the semi-circle with the radius 25cm, around the opening of the pipe and the radiation patterns are calculated from the mean square value of the pressure perturbation during one half of the signal period. The total simulated time is 2.8ms with the time step of around 0.25µs. Figure 3 shows the distribution of the pressure perturbation p_c' at one time instant (above) and the estimated radiation pattern shape (below) compared with the patterns from Figure 2 (below). As before, the mean flow properties are interpolated from the results of the CFD RANS simulations with the maximum Mach number value 0.25 and the temperature 300ºC. The Helmholtz number value is $He = 0.3$.

The upper figure clearly shows the small length scale pressure perturbations due to the vortices, which are successively generated and shed from the pipe edge inside the shear layer, as well as the large scale, low frequency acoustic perturbations, which are radiated in all directions.

The obtained radiation pattern shape, normalized according to the total energy, shows a fairly good match with the measurement results, with a somewhat more pronounced directivity. The discrepancy is probably due to the inaccuracy of the calculated mean flow profiles, especially in the zone close to the pipe edge, which is highly sensitive to the coarseness of the mesh. Still, by the inclusion of vortical modes, Linearized Euler Equations are capable of capturing accurately the far-field sound radiation from the pipe, but at substantial computational costs and with potential instability. On the other hand, the stable solution of convective wave equation (1), with the modelled effect of the vortices, seems to approach the measurement results with much less computational effort.

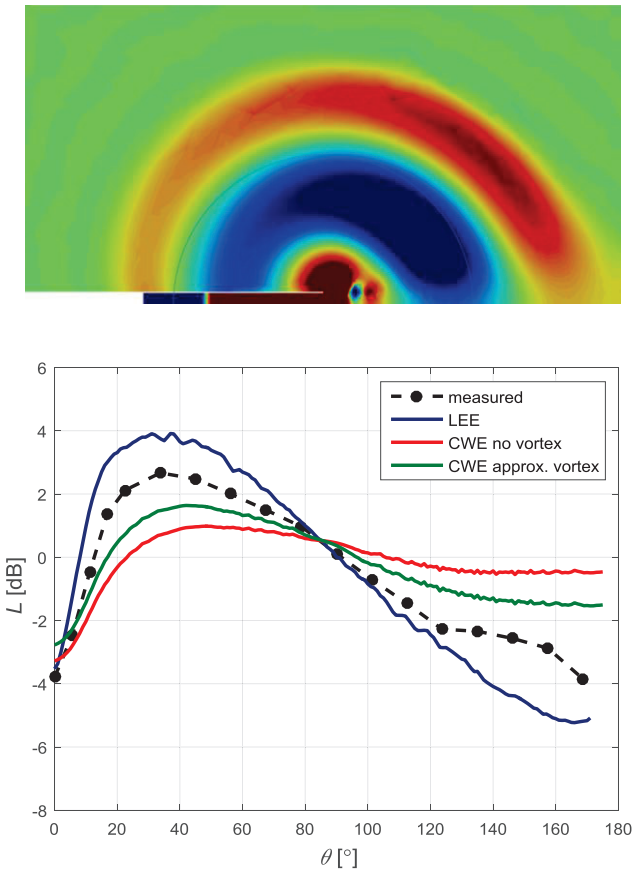

Figure 3: Distribution of pressure perturbation p_c' at one instant of time (above) and the calculated radiation pattern shape compared with the patterns obtained using convective wave equation and measurements (below); the blue line on the diagram above represents the arc on which the radiation pattern is acquired.

Conclusion

The paper presented a possible method for capturing the effects of the trailing edge on the far-field radiation of sound from an open unflanged pipe with a mean flow. Although the first results look promising, when compared to the computationally more demanding numerical solutions and measurements, the method has some obvious limitations as the vortex sound theory on which it rests. It is limited to low Mach and Helmholtz numbers. Its application for more complex geometries of the pipe opening, such as the ones of tail-pipes of vehicle exhaust systems, which can significantly increase the thickness of the shear-layer, should also be further investigated.

Literature

[1] Howe, M. S. Acoustics of Fluid-Structure Interactions. Cambridge University Press, 1998

[2] Hornikx, M., De Roeck, W., Desmet, W.: Flow and geometrical effects on radiated noise from exhausts computed by a hybrid extended Fourier PSTD method. 17th AIAA/CEAS Aeroacoustics Conference (32nd AIAA Aeroacoustics Conference), Portland, Oregon, (2011), AIAA Paper No. 2011-2844

[3] Hamiche, K., Gabard, G., Bériot, H.: A high-order Finite Element Method for the Linearised Euler Equations. Acta Acustica United with Acustica 102 (2016) 813-823

[4] Della Ratta Rinaldi, R., Iob, A., Arina, R.: An efficient Discontinuous Galerkin Method for aeroacoustic propagation. International Journal for Numerical Methods in Fluids 69 (2012) 1473–1495

[5] Ferziger, J. H., Peric, M., Computational Methods for Fluid Dynamics. Springer-Verlag Berlin, 2002

[6] Lilley, G. M.: On the noise from jets. Noise mechanisms. AGARD-CP-131 (1974) 13.1-13.12

[7] Doak, P. E.: Analysis of internally generated sound in continuous materials: 2. A critical review of the conceptual adequacy and physical scope of existing theories of aerodynamic noise, with special reference to supersonic jet noise. Journal of Sound and Vibration 25 (1972) 263-335

[8] Powell, A.: Theory of vortex sound. Journal of the Acoustical Society of America 36 (1964) 177-195

[9] Hesthaven, J. S., Warburton, T.: Nodal Discontinuous Galerkin Methods – Algorithms, Analysis, and Applications, Springer Science+Business Media, LLC, New York, 2008

Acknowledgments

The research work of Drasko Masovic has been funded by the European Commission within the ITN Marie Curie Action project BATWOMAN under the 7th Framework Programme (EC grant agreement no. 605867).

The authors acknowledge the financial support of the COMET K2 - Competence Centres for Excellent Technologies Programme of the Austrian Federal Ministry for Transport, Innovation and Technology (BMVIT), the Austrian Federal Ministry of Science, Research and Economy (BMWFW), the Austrian Research Promotion Agency (FFG), the Province of Styria and the Styrian Business Promotion Agency (SFG).